Macromolecules
ARTICLE

Macromolecules **2009**, *42*, 8451–8459 **8451**
DOI: 10.1021/ma901494z

Gelation Originated from Growth of Wormlike "Living Polymer" of Symmetrically Dendronized Large-Ring Crown Ether in Dilute Solutions

Jing-Jing Yan,[†] Ru-Pei Tang,[‡] Ben Zhang,[†] Xing-Qi Zhu,[†] Fu Xi,[‡] Zi-Chen Li,[†] and Er-Qiang Chen*,[†]

[†]*Beijing National Laboratory for Molecular Sciences, Department of Polymer Science and Engineering and Key Laboratory of Polymer Chemistry and Physics of Ministry of Education, College of Chemistry, Peking University, Beijing 100871, China, and* [‡]*State Key Laboratory of Polymer Physics and Chemistry, Joint Laboratory of Polymer Science and Materials, Institute of Chemistry, The Chinese Academy of Sciences, Beijing 100190, China*

Received July 10, 2009; Revised Manuscript Received September 1, 2009

ABSTRACT: The hierarchical pathway from homogeneous solution to gel of a large-ring crown ether symmetrically substituted with four first-generation Percec-type dendrons (**1**) in *n*-dodecane has been followed by differential scanning calorimetry (DSC), small-angle X-ray scattering (SAXS), and fluorescence anisotropy methods. The **1**/*n*-dodecane mixture requires a rather low gelation concentration of ~0.1% (w/v) at room temperature. Mainly on the basis of in situ thermal SAXS measurements, we have found that upon cooling from the homogeneous solutions of **1**/*n*-dodecane the **1** molecule first undergoes a solution self-assembly to form wormlike micelle with the core of crown ether and the shell of alkyl tails, which is "living polymers" containing only one disklike molecule of **1** per cross-sectional repeating unit. The driving force of the assembly can be mainly attributed to the reduction of free energy during microphase separation among the different regions of molecules with distinct chemical properties and the lipophilic−lipophobic interaction in the solvent that is selective for the alkyl tails. Growth of the "living polymer" proceeds continuously with lowering temperature and eventually brings the wormlike chains to entangle and to enter the miscibility gap of **1**/*n*-dodecane. We propose that phase separation of the "living polymer" solution is the main mechanism of the gelation, which gives a three-dimensional network of the slow-component of the "living polymer". The **1**/*n*-dodecane gel is "wet" with the solvent molecules participating in the "polymer"-rich phase. The lyotropic orderings of rectangular and nematic-like packing of the wormlike micelles can be obtained using slow and fast cooling protocol, respectively, which are very different from the hexagonal columnar phase found in the bulk and xerogel samples. We have also tested whether the channel formed by dibenzo-30-crown-10 moiety at the cylindrical micelle center of **1** can accommodate guest molecules. Using rhodamine B as an example, we have demonstrated that **1** can solubilize the cationic dye in *n*-dodecane at high temperature. After the micellization and gelation, the rhodamine B molecules are successfully introduced into the crown ether cavities.

Introduction

Gel is a kind of amazing soft material which has attracted enormous interests, not only because the gelation phenomenon is a fundamental problem in chemistry, physics, and life science but also with respect to the promised application in drug delivery, tissue engineering, filtration and separation, electronics, sensor, catalysts, etc.[1−9] However, as pointed out by Terech and Weiss, most of the current definitions of gel are largely descriptive and empirical.[5] The complex systems of gel possess astonishingly diverse molecular basis: the basic building blocks of gel can range from polymers to low molecular surfactants; the mechanism of gelation can be related to phase separation, aggregation and association of small particles, micellization, crystallization, chemical reaction, etc.; and the solvents can be either nonpolar or polar, depending on the properties of the gelators. Nevertheless, it is agreed that the essential structure of gel is a three-dimensional (3D) entangled network. With such a network, the gel containing a large volume of liquid can retain its shape and exhibit a solidlike rheological behavior. To completely understand the relationship between the chemical structure of gelator and the gel properties remains a challenging task so far. The elucidation of the inner structure of 3D network and the gelation mechanism will greatly help to rationally design new efficient gelators and to eventually make use of the gels.

As a typical physical gel, organogel based on low molecular weight organo-gelator (LMOG) has been paid much attention in the past decades. It usually requires a rather low concentration threshold of gelation (usually ≤2 wt %).[5] In contrast to the polymers with a topological preorder in at least one dimension (the chain structure), LMOGs can be viewed as zero-dimensional objects when they dissolve in solution. In order to form a 3D network, the small molecules must self-assemble solely based on noncovalent forces including solvophobic effects, hydrogen bonding, $\pi-\pi$ interaction, etc.[9] The network can be composed of fibers,[10,11] tapes,[12] platelets,[13] interconnected vesicles,[14] or spherulites.[15,16] Many researches reveal that the gelation of LMOGs can be ascribed to their crystallization in solution, which follows a mechanism of nucleation and growth.[8,15−18] In this case, the packing of LMOG molecules in both gel and bulk state shares a same structure. The LMOG crystal growth in solution is usually highly anisotropic; i.e., the growth favors one direction while along the other two directions the growth is pronouncedly

*To whom correspondence should be addressed. E-mail: eqchen@pku.edu.cn.

Published on Web 09/16/2009

Chart 1. Chemical Structure of Molecule 1

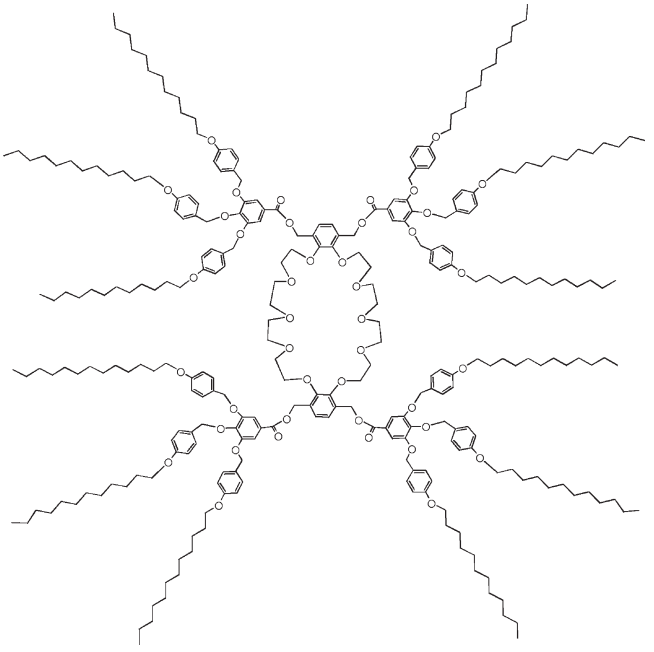

suppressed, resulting in LMOG fibers. In addition, frequently occurring fiber branching during crystallization can eventually give a 3D network. Liu and co-workers suggest that the branching, which is dependent on the supersaturation of solution, can be attributed to a crystallographic mismatch mechanism.[8,16] Therefore, controlling the crystallization condition of LMOG solution can conveniently lead to the control of morphology of fiber networks.[19−21]

If a LMOG lacks the crystallization ability or if its solution crystallization is greatly hampered, the molecular packing in the gel state may present a lyotropic organization, at least in the "junction zones" of the 3D network. The lyotropic microdomain composed of elemental fibers and solvent molecules may exhibit a packing symmetry the same as that found in the crystalline state of the LMOG, and the lyotropic lattice becomes more swollen with decreasing the LMOG concentration.[22,23] The gelator−solvent interaction may also change the packing symmetry of lyotropic phase. Terech et al. have reported that cholesteryl anthraquinone-2-carboxylate (CAQ) in decane forms a gel containing "junction zones" with hexagonal-like arrangement, but in mixtures of alkane/alcohol a more compact lamellar-like structure of CAQ develops progressively with increasing alcohol content.[22] Moreover, it is found that the solvent molecules can incorporate into the elemental fiber, leading to an increased fiber diameter.[23]

Compared with that caused by crystallization, gelation associated with lyotropic organization looks more complicated, which involves more hierarchical steps and depends on not only the chemical structure of the LMOG but also the interplay of the gelator−gelator and gelator−solvent interactions. It has been reported by Sakurai et al. that phase separation occurs prior to the appearance of lyotropic ordering.[11] Whitten et al. have traced the sol−gel transition process using a real space technique of atomic force microscopy (AFM).[24] After spreading a heated 1-octanol solution of a gelator containing a cholesterol moiety tethered to a *trans*-stilbene on a highly oriented pyrolytic graphite (HOPG) surface, they recorded sequentially the AFM images during gel formation. It is observed that fine fibers with a width of ~6.5 nm form at early stage, which continuously grow in one dimension and become dominate of the sol-phase droplets. Further condensation allows combination of the neighboring fibers into thicker ones, followed by forming a network with solvent molecules trapped inside the fiber bundles and even inside the elemental fibers. This visualization of gelation greatly helps us to understand the hierarchical steps of gelation in general. However, since a gelation-induced dewetting of the solution layer on the HOPG surface occurred, the sol−gel transition observed under AFM might not be exactly the same as that happened in bulk solutions.

In this paper, using a multiple-dendron-substituted crown ether as a model compound and mainly on the basis of the results obtained from the nondestructive in situ small-angle X-ray scattering (SAXS) thermal measurements, we intend to illustrate clearly the pathway of gel formation starting from the homogeneous solution to the final gel state with lyotropic organization. The LMOG molecule we studied (molecule **1**, see Chart 1) possesses a large-ring crown ether moiety at the center and four first-generation Percec-type dendrons linked to the crown ether in a rather symmetric fashion. Recently, many studies have revealed that dendritic molecules with various chemical structures can be effective LMOGs.[10,25−29] For instance, Aida et al. have reported that the dendritic LMOGs consisting of Fréchet dendrons and dipeptide (Tyr-Ala) moieties at the focal point can gel organic solvents at very low concentration (ca. 1.0 mM).[28,30] The reason we chose the Percec-type dendron to construct a LMOG molecule roots in its self-assembling behavior found in both bulk[31−36] and solutions.[37,38] Among many fascinating mesophase structures,[31,39−41] it is worth noting that the wedge-shaped Percec-type dendrons can assemble into liquid crystalline columnar (Φ) phases with the building block of columns formed by stacking the dendrons. While a long-range two-dimensional positional order of the column packing can be observed on the nanometer scale, on the subnanometer scale the positional order is usually absent mainly due to the fact that the flexible alkyl tails and semiflexible aromatic portions of the dendrons possess remarkable interior freedom.[35,38,42] In this context, we expect that the molecules with Percec-type dendrons can be good candidates for LMOG; namely, the molecules favor a unidimensional assembly to form a cylindrical entity, but the crystallization is largely prevented. It has been reported by Beginn et al. that a Percec-type dendron with a benzo-15-crown-5 group at the focal point can gel acrylate solvents.[37,43] Recently, Percec et al. have synthesized a series of LMOG with the linker between two Percec-type dendrons containing amide groups. The twin-dendritic molecules demonstrate the effective gelation ability toward a broad range of solvent polarities, and moreover, some of the gels exhibit unique thixotropic properties.[38]

Herein we focus on the gelation mechanism of molecule **1** in *n*-alkane solution. When adopting an unfolded conformation, the molecule is more or less disklike as a whole. We find that upon cooling from homogeneous solution the molecules first stack to form wormlike micelles with the core of crown ether groups. Most likely, the micelle contains only one disklike molecule per cross-sectional repeating unit, which belongs to the simplest case of molecular threads. Moreover, it is a typical "living polymer",[44] of which the length increases with decreasing temperature. According to the experimental observation, we consider that the sol−gel transition is mainly induced by the solution phase separation after the "living polymers" become sufficiently long and entangled.[3,45,46] In the "polymer"-rich phase, the wormlike micelles may pack into either a lyotropic rectangular Φ or a sort of nematic phase, depending on the cooling rate applied is slow or fast, respectively. The SAXS result clearly indicates that the packing symmetry of lyotropic phases is very different from that observed in solid state or xerogel of **1**.

We have purposely introduced a large-ring crown ether moiety to **1**, which will not only impart great adjustability to facilitate gelation[47−49] but also provide additional functions.[50,51] Crown

ethers can selectively complex with a variety of cations such as alkali metal cations and ammonium cations.[52] For the wedge-shaped Percec-type dendron functionalized with benzo-15-crown-5 at the focal point, the crown ether groups stack unidirectionly into a hydrophilic cavity at the center of the columns, which may mimic the natural ion channels such as those formed by Gramicidine A.[35] For **1** with four symmetrically substituted Percec-type dendrons, we suspect that a similar molecular channel can be constructed, and after gelation, such a channel coexists with the porous structure with a sub-micrometer cellular size that naturally exists in gels. The dibenzo-30-crown-10 moiety in **1** is relatively large, providing a cavity big enough to accommodate larger ions such as Pb^{2+} and molecular species such as bipyridium ions and aromatic ammonium ions.[53−56] Using rhodamine B as the guest molecule, our preliminary result indicates that **1** can solubilize the cationic dye in nonpolar alkane solvents. After micellization and gelation the rhodamine B molecules are successfully included in the crown ether channels with a significantly reduced rotational diffusion.

Experimental Section

The synthesis of **1** is described in detail in the Supporting Information. In brief, the dendrons and the crown ether core were synthesized separately, and then the dendrons were coupled to the crown ether core in a molar ratio of 4:1 through esterification. **1** was characterized by standard spectroscopic methods, which gave satisfactory data corresponding to its expected molecular structure (see the Supporting Information).

To prepare the gel sample, **1** was placed in a capped vial, and a proper amount of *n*-alkane such as *n*-hexane and *n*-dodecane was added. In this paper, we focus on the mixture of **1**/*n*-dodecane. The mixture was heated to 100 °C in oil bath for 10 min and was then cooled to room temperature. The gelation temperature (T_{gel}) was determined by the test-tube-tilting method as described in the literature.[57] Xerogel samples were obtained by slow evaporation of solvent under dynamic vacuum at around 10 °C.

The morphology of xerogel of **1** was examined using AFM (DI NanoScope IIIa) and transmission electron microscopy (TEM, a JEM-200CX). For AFM observation, the gel sample was transferred onto freshly cleaved mica surfaces by gently withdrawing the mica sheets which were immersed in a newly formed gel. After the samples were dried, the AFM height and phase images of xerogel were recorded using taping mode, wherein the cantilever force was controlled to be large enough to explore the surface feature yet small enough to avoid sample damage. TEM experiments were performed with an accelerating voltage of 120 kV. The xerogel samples on copper grids precoated with a thin film of Formvar were prepared using a method similar to that for AFM experiments, and no further staining was applied to the samples.

Differential scanning calorimetry (DSC, Mettler-Toledo DSC821e) equipped with a high-sensitivity sensor (HSS7) was utilized to study the thermal behavior of the **1**/*n*-dodecane mixture upon cooling and heating at a rate of 10 °C/min. The mixture with a concentration of 1.0% (w/v) and weight of ~80 mg was carefully encapsulated in the hermetically sealed aluminum liquid pan.

Scattering of **1**/*n*-dodecane mixture was examined using a high-flux SAXS instrument (SAXSess, Anton Paar) equipped with a Kratky block-collimation system and an imaging plate (IP) as the detector. Since the IP with a pixel size of $42.3 \times 42.3\ \mu m^2$ is extended to high-angle range (the q range covered by the IP is up to $29\ nm^{-1}$, $q = 4\pi \sin\theta/\lambda$, where the λ is the wavelength of 0.1542 nm and 2θ the scattering angle), both SAXS and wide-angle X-ray scattering profiles can be simultaneously recorded. The scattering peak positions were calibrated with silicon powder for wide-angle region and silver behenate for small-angle region, respectively. A temperature control unit (Anton Paar TCS-120) in conjunction with the SAXSess, which can control the temperature in the range of −20 to 120 °C with an accuracy of 0.1 °C, was utilized to study the structure evolution of **1**/*n*-dodecane as a function of temperature.

We carefully loaded the solution samples for SAXS measurement into a quartz capillary with a diameter of 1 mm after the 1.0% (w/v) **1**/*n*-dodecane was heated to be a clear solution. To prevent gelation during the solution injection, the capillary was also preheated to above 50 °C. The scattering profiles were recorded upon cooling from 70 to 10 °C. The sample was allowed to equilibrate for 1 h at each set temperature before measurement. The exposure time of 1 h was found to be enough long to give a good signal-to-noise ratio. The scattering curve of pure *n*-dodecane filled in the same capillary was measured as the background. After background subtraction, desmearing was performed according to Lake's method.[58] The pair-distance distribution function (PDDF) of scattering curves above the T_{gel} was calculated using the generalized indirect Fourier transform (GIFT)[59,60] program included in the SAXSess software package. For comparison, we also recorded the scattering pattern of the xerogel and bulk samples of **1** at room temperature. The dry powders were wrapped by aluminum foil and then fastened on the sample holder, and the exposure time was 15 min.

To test whether **1** in *n*-dodecane can solubilize the cationic dye of rhodamine B, we carried out the measurements of UV−vis and fluorescence spectra. The concentration of rhodamine B in solutions was 2.5×10^{-6} mol/L. The homogeneous dispersion of rhodamine B in **1**/*n*-dodecane was prepared by adding dropwise 20 μL of ethanol solution of rhodamine B (2.5×10^{-4} mol/L) into 2 mL of 0.1% (w/v) **1**/*n*-dodecane mixture at around 70 °C under vigorous stirring. After the addition, the mixture was further stirred at 40 °C under gentle N_2 flow for 2 h to remove the residue ethanol.

The UV−vis absorption spectra were recorded using a Varian Cary 1E UV−vis spectrometer with the solvent as reference. The steady-state fluorescence spectra and excitation fluorescence anisotropies were measured on a Varian CARY Eclipse fluorescence spectrometer. For rhodamine B, the excitation and emission spectra were detected at $\lambda_{em} = 615$ nm and $\lambda_{ex} = 520$ nm, respectively, using slits with band-pass of 5 nm for both monochromators. To determine fluorescence anisotropies, the filter polarizers of the spectrometer were aligned in L-format configuration. The excitation anisotropy value r was calculated from $r = (I_{VV} - GI_{VH})/(I_{VV} + 2GI_{VH})$, where I_{VV} and I_{VH} are the fluorescence intensities polarized parallel and perpendicular to the excitation light at $\lambda_{em} = 615$ nm, respectively, and G is the instrumental correction factor of I_{HV}/I_{HH}. For pure **1** in *n*-dodecane [0.1% (w/v)], the steady-state excitation fluorescence anisotropy spectra were recorded at $\lambda_{em} = 365$ nm, which corresponds to the emission maximum of the phenyl groups in the dendrons. Since the fluorescence is rather weak, the slit band-pass was 10 nm for both monochromators.

Results and Discussion

Gelation and Thermal Behavior of 1 in *n*-Dodecane. At the molecular structure level **1** bears several regions with distinct chemical characteristics, i.e., the crown ether core, the aromatic region, and the outer portion consisting of dodecyl tails, which are incompatible with each other and tend to separate. Therefore, the molecule in the solvents which are selective for one of the three regions can be expected to undergo solution assembly, resulting in a structure with the solvophilic and the solvophobic moieties occupying the surface and the inner part, respectively. In this research, we choose *n*-alkane (particularly *n*-dodecane), which is good for the dodecyl tails and poor for the aromatic rings and the crown ether moiety, as the selective solvent. We found that **1** could be well dissolved in *n*-alkanes at high temperature. For example, the solid powders completely disappeared in *n*-dodecane at 70 °C after vigorous stirring or sonication. The **1**/*n*-dodecane mixtures became gels at room temperature, with

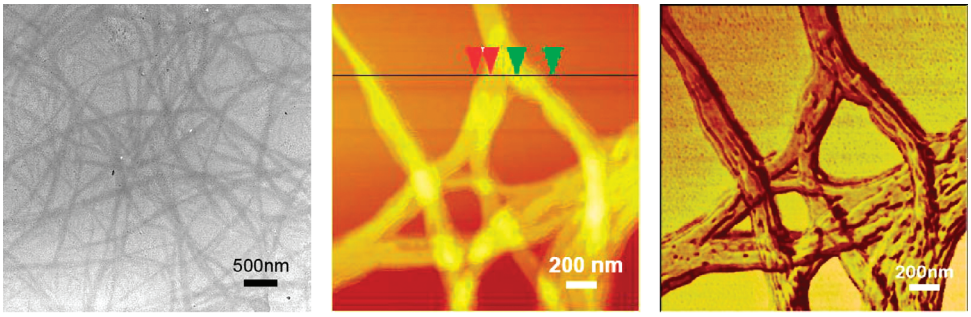

Figure 1. TEM (a) and AFM [(b) for height and (c) for phase] images of xerogels. The concentration of the **1**/*n*-dodecane was 0.2% (w/v). In (b), the height differences between the two red arrows and the two green arrows are 7.4 and 11.7 nm, respectively.

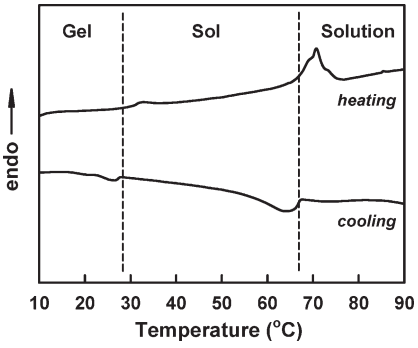

Figure 2. DSC thermal diagrams of a **1**/*n*-dodecane mixture [1.0% (w/v)] recorded during cooling and subsequent heating at a rate of 10 °C/min.

a gelation threshold as low as 0.1% (w/v). Upon cooling, the mixture remained transparent until approaching 30 °C when the Tyndall effect became more and more obvious. The solution turned to be gel at below 30 °C. The gels were translucent when the concentration exceeded 0.25% (w/v). On the basis of the simple visual test of the nonflowing character in a test-tube-tilting method, the T_{gel} was measured to be increased from 25 to 30 °C when the concentration was varied from 0.1 to 2.0% (w/v). The gels were rather "weak"; i.e., mildly shaking the test tubes would result in the gel breakage. After it was heated to above the T_{gel} followed by cooling again, the gel could recover readily, indicating that **1** was a typical thermal-reversible physical LMOG.

The morphology of the xerogels on copper grids and freshly cleaved mica surfaces were investigated under TEM and AFM, respectively. Both the TEM and AFM images (Figure 1) show interwined fibers with the length of many micrometers, reflecting that the molecules had assembled into a 3D network in the gel state. The width of the fibers varies from tens to hundreds of nanometers, whereas the height measured by AFM is usually of 5−20 nm (see below the discussion). The divergences are frequently observed along the fibers, which is especially clear in the AFM phase image (see Figure 1c), indicating that the fibers are actually consisted of finer fibrils. For different concentrations, the morphologies are essentially the same except that the density of assemblies and the bundle size of the fibrils increased with concentration.

In order to follow the whole assembly process of **1** in *n*-dodecane, we performed thermal experiments of DSC and SAXS using the samples with a concentration of 1.0% (w/v) which could give enough high signal-to-noise ratios. Figure 2 describes the DSC traces of the mixture recorded during the cooling and subsequent heating at a rate of 10 °C/min. Two

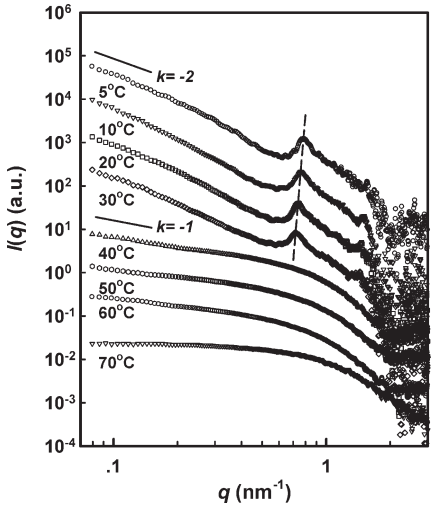

Figure 3. A set of SAXS profiles of 1.0% (w/v) **1**/*n*-dodecane measured at different temperatures upon cooling. The desmeared profiles are moved vertically for clarity.

transitions, which are enantiotropic, are observed in the temperature range of 10−90 °C. The onset temperatures of the transitions measured from cooling and heating are rather close to each other, indicating that the transitions are close to equilibrium. The low transition temperature at ∼29 °C is consistent with the T_{gel} measured using the test-tube-tilting method, which suggests that this transition is largely related to the sol−gel transition of the mixture. On the other hand, the transition at high temperature with much large latent heat (nearly 14 times of the low one, see below the discussion) appears at ∼68 °C. This implies that in a wide temperature window between the two transitions a sort of molecular self-assembly exists in a sol state. As the solid sample of **1** could be well dissolved in *n*-dodecane at above 70 °C, we consider that the **1**/*n*-dodecane shall become a true solution after the transition at high temperature.

As been proven to be a powerful and nondestructive method, X-ray scattering has been widely used to explore the structure of organogels.[11,22,23,61,62] Figure 3 depicts our SAXS profiles (log $I(q)$ vs log q) of **1** in *n*-dodecane [1.0% (w/v)] measured at various temperatures during cooling. Compared to that recorded at lower temperatures, the scattering curve at 70 °C with the intensity decay starting at a much higher q value is typical for homogeneous solution, meaning that the particles therein possess a smaller size. Once the temperature is lowered to 60 °C, the low-angle scattering intensity increases significantly, and moreover, a slope of −1 for the initial intensity decay can be identified. The scatterings at 50 and 40 °C share

the feature same as that observed at 60 °C. However, when further lowering the temperature to 30 °C and below, a set of scattering peaks appear at high q region ($q > 0.6$ nm^{-1}) accompanying the initial intensity decay slope becomes nearly −2. Combining the DSC and SAXS results, we can divide the whole temperature range of the transitions of the **1**/*n*-dodecane mixture into three regions, i.e., >∼70 °C for the solution, 30−70 °C for the sol, and <∼30 °C for the gel. To understand clearly the assembly and gelation process, we will analyze the SAXS data in great detail.

Wormlike "Living Polymer" in the Sol State. At above the T_{gel} of ∼30 °C, the SAXS profiles in Figure 3 exhibit monotonic intensity decay. Since the system with a low concentration of 1.0% (w/v) remains a clear solution and there are no scattering peaks observed, it is reasonable to assume that the scattering is mainly attributed to the form factor. Therefore, the asymptotic behavior of $I(q) \sim q^{-1}$ observed in the low-angle region at 40−60 °C strongly suggests that the particles in solution are cylinder-like.[63,64] To further evaluate the particle shape and dimensions, we calculated the PDDFs from the fitting of the scattering curves using the model-free method of GIFT.[59,60,65] The results are described in Figure 4, where the PDDF of 70 °C is also presented for comparison. The crossover of the decay of PDDF curve with the abscissa (r-axis) reflects the maximum dimension of the particle (e.g., the length of cylindrical particle). Clearly, the largest dimension is about 6 nm at 70 °C. Therefore, no large aggregate exists; namely, the **1** molecules are dissolved in the solution as unimer. In contrast, for the lower temperatures, the intercept at the abscissa shifts dramatically to $r > 20$ nm. Moreover, the nearly triangle-shaped PDDFs are typical for rodlike particles, of which the inflection in the decay part of the PDDF curve (indexed by the vertical dashed line) gives a rough estimate of the diameter of the rod cross section (d_C). The d_C values remain a constant of ∼5 nm for 60, 50, and 40 °C, indicating that the structures of the rodlike particles are essentially the same despite varying temperature in the sol state.

Considering the chemical structure of **1**, the large-ring crown ether with significant flexibility may adopts either a folded or an unfolded conformation.[14,49] As the SAXS result evidence the rodlike assembly of **1**, we consider that the molecules are disklike with unfolded crown ether moiety, which can stack parallel to each other and thus form rod or cylinder with the core of crown ether groups and the shell of alkyl tails. We believe that the lipophilic−lipophobic balance plays a critical role in the solution self-assembly of **1**. The solubilities of the three distinct regions in **1** molecule are rather different in *n*-dodecane that is selective for the dodecyl tails. As the two inner components become more soluble at higher temperature, **1** can be dissolved in *n*-dodecane. When the temperature decreases, the aromatic and crown ether moieties with reduced solubilities tend to aggregate. Consequently, the outer dodecyl shell of resultant rodlike or cylindrical micelle can protect the solvophobic components.

For the SAXS experiments, the dodecyl tails of **1** in *n*-dodecane shall be "invisible" due to the effect of electron density matching. Therefore, the diameter measured by SAXS should mainly correspond to that of the solvophobic cores, of which the diameter is ∼1 nm smaller than that of the cylinders read off from the PDDFs (∼5 nm). This infers that the longitudinal fluctuation of the molecular position, which is naturally caused by the thermal energy, exists along the cylinder, resulting in apparently a large diameter. For the assembly of **1** in *n*-dodecane, there is no specific interaction between the molecules introduced. Although the $\pi-\pi$ stacking of the aromatic rings is involved (see the Supporting Information), the intermolecular interaction is not sufficient strong to hold the molecules of **1** at strict positions within the assembly. In this context, the cylindrical micelles are wormlike with a certain degree of flexibility.

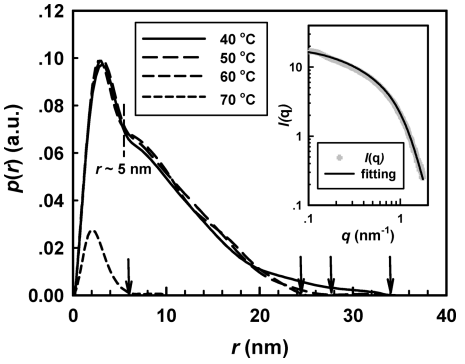

Figure 4. PDDFs [$p(r)$] of 1.0% (w/v) **1**/*n*-dodecane at 40, 50, 60, and 70 °C. The arrows indicate the intercepts at the abscissa for the various temperatures. As an example of 50 °C, the inset shows the GIFT simulated curve (solid line) fits well the raw scattering data (gray dots).

The wormlike micelle of the **1** is in fact a simple "living polymer" with only one molecule per cross-sectional repeating unit. In Figure 4, we note that the decay of PDDFs extends to larger r with decreasing temperature. As indexed by the arrows, the intercept which is the representative of the cylinder length locates at $r \approx 25$ nm for 60 °C, which moves to $r \approx 28$ nm for 50 °C and 34 nm for 40 °C. Moreover, the final decays of the PDDFs are not very linear, indicating that the cylinder length is not uniform but possess a distribution. Because of the detection limit in our equipment ($q_{min} \sim 0.08$ nm^{-1}, i.e., $d_{max} \sim 40$ nm), the cutoff at low q-region may affect the calculated PDDF, and therefore, the length of the cylinder at low temperatures may be underestimated. However, the trend of increasing length with decreasing temperature is reliable, which is associated with the growth of the "living polymer" or the increase of "degree of polymerization" (DP). Thermodynamically, the DP is determined by the equilibrium between the "living polymer" and unimer. For the solution assembly of **1** mainly driven by the solvophobic interaction, lowering temperature shifts the equilibrium toward forming longer chains. Such an increase of the length has been reported for several cylindrical micelle systems.[66] We presume that the growth of "living chain" will finally lead to the gelation of **1**.

Lyotropic Ordering in the Gel State. Compared with those recorded at above 30 °C, the SAXS profiles at lower temperatures are remarkably changed in two aspects: one is that in the double-logarithmic plot the slope of initial decay becomes nearly −2 instead of −1, and another is the emergence of diffraction peaks at $q > 0.6$ nm^{-1}. The low-q asymptotic behavior of $I(q) \sim q^{-2}$ is indicative of the scattering entities with the lateral dimensions much larger than the thickness, such as lamellae or ribbonlike fibers, which are very different from the one-dimensional cylinders. In addition, the diffractions reflect a sort of ordered structure of molecular packing within the aggregates. Because the wormlike "living chains" are formed *prior to* the gelation, we consider that their packing shall be responsible for the lyotropic ordering observed in the gel state.

For the gels with low concentrations, it is usually difficult and even impossible to precisely identify the ordered packing of the gelator molecules on the basis of only a few observable diffractions. Nevertheless, a rational analysis may help to understanding the gel structure. In Figure 3, two of the peaks at $q = 0.72$ and 1.43 nm^{-1} are obvious at 30 °C, which follows

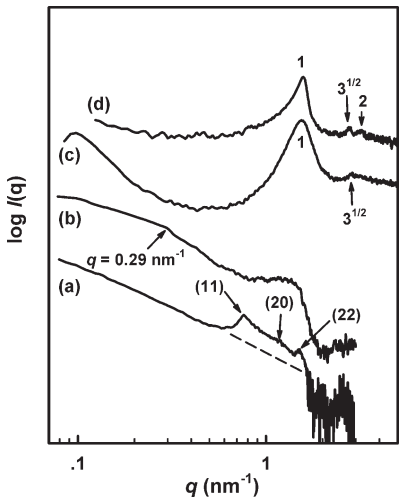

Figure 5. Comparison of SAXS profiles obtained from different samples: (a, b) gels at 10 °C after step-cooling and quenching from 70 °C, respectively; (c) xerogel dried from **1**/*n*-dodecane; (d) bulk powder of **1**.

the ratio of nearly 1:2. Moreover, a weak and broad peak located in the vicinity of $q = 1.0$ nm^{-1} is also observed. As shown by the enlarged pattern acquired at 10 °C in Figure 5, this broad peak, which is obviously above the baseline (schematically shown by the dashed line), can be recognized clearly. Because the q ratio of the peaks significantly deviates from the theoretical sequence of hexagonal packing, we attempted to index the peaks with a centered rectangular two-dimensional (2D) lattice (space group of *cmm*) of lyotropic columnar mesophase with the cylindrical micelles as the elemental units. The strongest peak can be assigned to the (11) diffraction from the close packing plane. The (20) and (02) diffractions may overlap to form the broad peak; we simply assume that the peak maximum position to be that of the (20) diffraction. This indexing corresponds to a rectangular cell with $a \approx 11$ nm and $b \approx 13$ nm (the schematic draw is depicted in Figure 6). The difference between a and b may be due to that the cylinders in the 2D lattice are not perfectly circular but rather ellipsoidal. This may further cause nonequivalent dimensions of the fiber along the a and b direction. Consequently, the lyotropic domains (the fibers in the gel state) can be ribbonlike with a largely asymmetric rectangular section; i.e., the thickness is much smaller than the width. In this case, the low-q asymptotic behavior of $I(q) \sim q^{-2}$ is observed.

Of particular interest is to compare the diffractions acquired from the gel with that of the bulk sample. As shown in Figure 5, the first diffraction peak of the bulk (curve d) appears at a significantly higher q position in comparison with that of the gel obtained after slow cooling. Similar to that found in many other molecules with Percec-type dendrons, the q ratio of the three bulk diffractions follows $1:3^{1/2}:4^{1/2}$, evidencing a well-ordered hexagonal lattice with $a = b = 3.91$ nm. Therefore, **1** in bulk presents a hexagonal columnar liquid crystal (Φ_H) phase, wherein the columns with a diameter of 4.52 nm are constructed by parallel stacking of the disklike molecules. This comparison tells that the packing behaviors in bulk and in gel are quite different, although for both cases the building blocks are all the **1** cylinders. For the rectangular lattice in the gel state, half the cell dimension is larger than the cylinder diameter of **1** packed in the bulk Φ_H phase. Although the shells of the alkyl tails are "invisible" in the form factor of micelles (in the PDDFs), they now become indirectly "visible" in the gel state because they keep neighboring wormlike micelles apart from each other. However, note that the amount of space between the separated solvophobic cores of micelles cannot be fully filled by the alkyl tails themselves. In this case, the solvent molecules must participate in the formation of lyotropic mesophase, which swell the shell layers of alkyl tails and thus the micelle packing. Therefore, the gel of **1**/*n*-dodecane belongs to the category of "wet gel".[11,24,67] As the temperature decreases, the diffractions of the gel continuously shift to high q values (indicated by the dashed line in Figure 3). The (11) d-spacing decreases by nearly 9% from 30 to 5 °C, which shall be mainly attributed to that the solvent is expelled from the shell layer. Complete removal of solvent between the cylinders can dramatically alter the packing structure and the fiber morphology as well. As shown by curve c of Figure 5, the diffraction pattern of the **1**/*n*-dodecane xerogel renders the feature same to that of the bulk, indicating that the rectangular packing is relaxed to the Φ_H phase. The first-order diffraction of the xerogel peaks at a q value just slightly lower than that of the bulk, inferring that the dried sample may contain residual *n*-dodecane. Furthermore, one can expect that the rectangular structure of the "wet gel" gradually collapsed during drying on solid substrates, which would result in the fibers in xerogel with greatly reduced thickness. Therefore, the height of the ribbonlike fibers measured from AFM image (see Figure 1) in fact gives an underestimation of the fiber thickness in the gel state. Here, our result also suggests that using the scattering profile and AFM height image of xerogel to deduce the packing mode and fiber dimension in the wet gel, which is widely applied in current research, is not always convincible.

Mechanism of the Gelation of 1/*n*-Dodecane. The **1**/*n*-dodecane "wet gel" is composed of two phases, wherein the **1**-rich phase with lyotropic organization constructs the 3D network. Sakurai et al. have reported that during cooling from a homogeneous solution of methyl 4,6-*O*-benzylidene-α-D-mannopyranoside/*p*-xylene, phase separation takes place initially, and subsequently the hexagonal lyotropic organization is developed within the solute-rich phase.[11] For the **1**/*n*-dodecane, it is also interesting to ask whether the phase separation resulted from the ordered packing of wormlike cylinders of **1** or, similar to that reported by Sakurai, the lyotropic phase is formed after solution phase separation. If the latter is the case, we shall ask what can be the main factor responsible for the phase separation.

To elucidate the interplay of phase separation and lyotropic organization, we further investigated the structure of gel sample prepared by fast cooling or quenching. Fast cooling may result in a wide length distribution of the wormlike "living polymer" and may at least partially hamper the formation of ordered lyotropic phase. Therefore, the system does not reach the equilibrium state. In Figure 5, we depict a SAXS curve of a gel sample obtained by cooling from 70 to 10 °C within ~5 min. It is intriguing that, instead of a set of diffraction peaks, an amorphous halo appears in the q-range of 0.8−1.8 nm^{-1}. Moreover, in the decay part of $\log I(q) \sim \log q$ a kink at $q = 0.29$ nm^{-1} is observed, which may reflect the average lateral size (~22 nm) of the fibers in the gel.[68] The amorphous halo shall be mainly contributed from the scattering of mixed long and short wormlike micelles of the **1** within the fibers.[69] We presume that the long ones preferentially orient along the fiber direction but lose their 2D positional order; namely, the micelles pack together in a sort of nematic fashion. In this case, the maximum position of the halo with a dimension of ~5 nm, which is apparently consistent with the diameter of the wormlike micelles, may correspond to the average distance between two adjacent parallel micelles. Compared with that

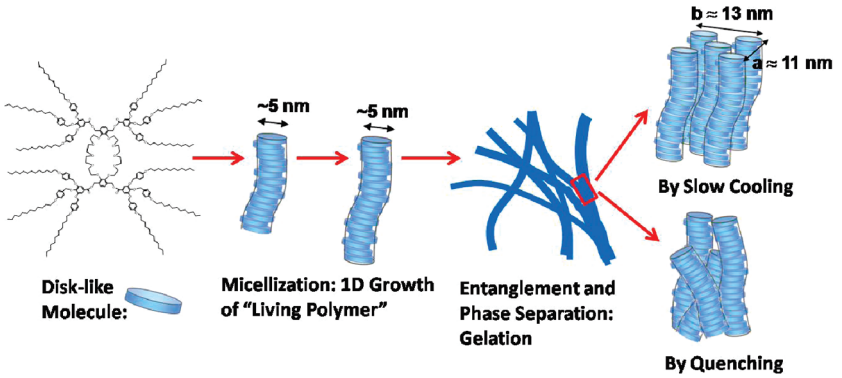

Figure 6. Schematic illustration of the hierarchical steps toward the gel of **1** in *n*-dodecane upon cooling.

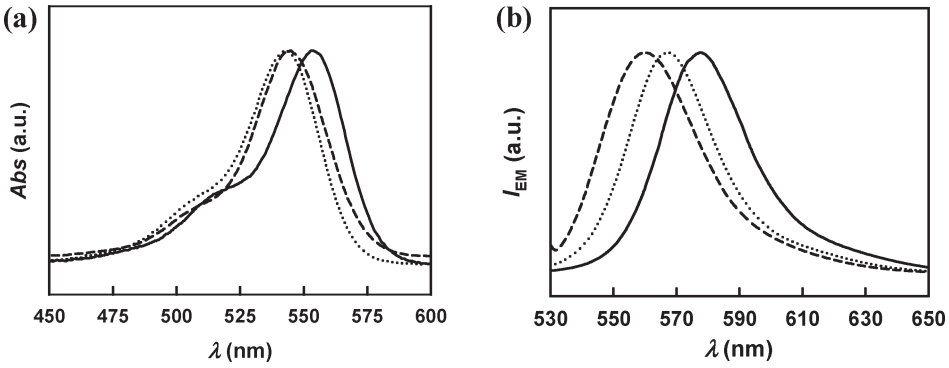

Figure 7. UV−vis absorption and fluorescent emission spectra of 2.5×10^{-6} mol/L rhodamine B in water (solid), ethanol (dotted), and 0.1% (w/v) **1**/*n*-dodecane (dashed) at room temperature.

of well-developed wormlike micelles packed in a rectangular structure, the gel prepared by a rapid cooling protocol shall be metastable. Its existence indicates that the formation of highly ordered lyotropic phase is not a prerequisite for the gelation.

Therefore, we propose that the gelation of **1**/*n*-dodecane is more related to the phase separation of the sol containing entangled "living chains". As aforementioned, lowering temperature favors to form longer "living polymer" of **1**. Such a growth mode resembles that of cylindrical or wormlike micelles (also "living polymers") frequently observed in aqueous systems such as cationic surfactant/water[44] and PEO−PPO−PEO (Pluronics)/water,[70,71] and it is also found in a lecithin/isoctane reverse micelle system which contains a small content of water.[45,72] Those "living polymers" are in a balance with the unimers, and decreasing temperature or increasing concentration both can cause micelles to increase in length and finally to form gel.[45,73] We suggest that the "living polymer" system can possess an upper critical solution temperature (UCST). Continuous growth of the length of the **1** "living polymer" will lead the chains to be entangled, wherein the system is reminiscent of semidilute polymer solutions. More importantly, this process also moves upward the binodal line of the phase diagram. Eventually, the sol of **1**/*n*-dodecane enters the miscibility gap. Since the giant wormlike "living polymer" bears a dynamics much slower than the solvent, a viscoelastic phase separation can result in the gel state with a bicontinuous phase.[3] This gelation pathway from homogeneous solution to gel state is depicted schematically in Figure 6. In the "living polymer"-rich domains, either the ordered rectangular or the nematic-like packing will be further developed depending on the cooling protocol. Since the solution phase separation dominants the gelation, the latent heat of gelation is much smaller than that of forming "living polymer" which requires the intimate interaction between the molecules (see Figure 2).

Inclusion of the Guest Molecule of Rhodamine B. It is of particular interest to examine whether the cylindrical micelle or column of **1** with the crown ether groups located at the center portion can render a functionality of loading and even transporting guest polar molecules. Note that the supramolecular column of **1** bears only one molecule (i.e., one crown ether ring) per repeating unit. Therefore, the hydrophilic channel contains fewer encumbrances inside in comparison with other similar channels composed of several crown ether rings per repeating unit. Moreover, the large ring of dibenzo-30-crown-10 provides a cavity to include relatively large molecules, especially those which can specifically interact with the crown ether moiety.

We choose rhodamine B as the guest molecule. This cationic dye has an extremely low solubility in pure *n*-dodecane. Its characteristic UV−vis absorption and fluorescent emission were hard to be detected from the saturated *n*-dodedane solution obtained by longtime vigorous stirring or ultrasonic agitation. However, the dye molecule can be homogenously dispersed in **1**/*n*-dodecane with the molar ratio of rhodamine B to **1** up to ~5%. Figure 7 displays the UV−vis absorption and steady-state fluorescence spectra of rhodamine B (2.5×10^{-6} mol/L) in a 0.1% (w/v) **1**/*n*-dodecane measured at room temperature. For comparison, the spectra measured from the dye solutions of water and ethanol are also given in Figure 7. The homogeneous dispersion of rhodamine B in **1**/*n*-dodecane was obtained by gradually dropping an ethanol solution of rhodamine B into **1**/*n*-dodecane at around 70 °C under vigorous stirring followed by further removing ethanol with a gentle flow of N_2 purge gas at 40 °C. The successful removal of ethanol can be confirmed by the fluorescent spectra (Figure 7). Compared

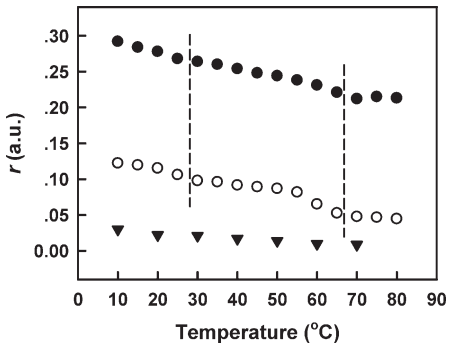

Figure 8. Fluorescent anisotropies (r) of rhodamine B (solid circle) and **1** (open circle) in 0.1% (w/v) **1**/*n*-dodecane mixture and rhodamine B in ethanol (triangle) at various temperatures measured during cooling. The concentration of rhodamine B is 2.5×10^{-6} mol/L.

with that of 567 nm measured from the ethanol solution, the emission maximum of rhodamine B in **1**/*n*-dodecane appears at 560 nm. This blue shift also reflects that the dye molecules in **1**/*n*-dodecane are subjected to a less polar microenvironment, which shall be associated with the crown ether cavities. It has been reported that cationic dyes such as rhodamine B can interact with the short poly(ethylene glycol) (PEG) chain within nonionic surfactants such as Triton X-100 through charge-transfer interaction.[74,75] Such type of interaction shall also exist between the electron-rich crown ether ring and the ammonium ion of rhodamine B. Consequently, solubilization of rhodamine B in the mixture with majority of *n*-dodecane can be achieved.

We further carried out fluorescence anisotropy measurements of rhodamine B in **1**/*n*-dodecane and of pure **1**/*n*-dodecane at various temperatures. The results are shown in Figure 8. In order to reduce as much as possible the effect of scattered light which can lead to artificially high fluorescence anisotropy, the concentration of **1** in *n*-dodecane was chosen to be 0.1% (w/v), where a clear transparent gel could be obtained. For the pure **1**/*n*-dodecane, the r values at $\lambda_{ex} = 317$ nm and $\lambda_{em} = 365$ nm measured upon cooling demonstrate three distinct temperature regions, consistent with that observed in our DSC and thermal SAXS experiments. At above 65 °C, the r value of the phenol group remains nearly a constant of ~0.05, which is reasonable for the free **1** molecules in solution. Upon cooling to below 65 °C, the r value increases significantly, indicating the formation of wormlike "living polymers" that prolongs the molecular rotational correlation time. This micellization process proceeds with further cooling, and the r value reaches a plateau at below 50 °C. Finally, a second increase of r appears when the sol−gel transition occurs at around 30 °C, which is associated with the further slowdown of the rotational diffusion in the gel state.

We find that the r values at $\lambda_{ex} = 520$ nm and $\lambda_{em} = 615$ nm for rhodamine B in **1**/*n*-dodecane present the temperature dependence identical to that observed for the pure **1** in *n*-dodecane. This result infers that the rhodamine B molecules are included in the wormlike micelles, and moreover, the existence of guest molecule does not alter too much the assembly behavior of **1** in *n*-dodecane. Compared with an r value of ~0.02 measured from an ethanol solution (see Figure 8), the r value of ~0.22 of rhodamine B in **1**/*n*-dodecane at above 65 °C is extremely high. Although the effect of scattered light might not be completely eliminated in our measurement, we consider that the high r values still reflect that the rhodamine B molecules are not free in the solution at high temperatures. Most likely, before the **1** molecules form micelles, a rhodamine B molecule is surrounded by a few **1** molecules, forming a "cluster" with a significantly reduced rotational diffusion. In this case, the cationic dye with a very poor solubility in *n*-dodecane can avoid precipitation and thus can be dispersed homogenously. The same trends of the fluorescence anisotropies varying with temperature observed for both the rhodamine B and **1** molecule suggest that the motion of the dye molecules is tightly related to the assembly of **1** molecules upon cooling. Namely, once the **1** molecules form wormlike micelles, the dye molecules in the "clusters" will be brought into the crown ether cavities at the micelle center and remain therein afterward. The diffusion along the crown ether channels of the confined rhodamine B molecules was not examined yet, which shall be tackled in the near future.

Conclusions

In this paper, the detailed hierarchical steps toward gel state of a large-ring crown ether symmetrically substituted with four Percec-type dendrons (**1**) in *n*-dodecane has been studied. Upon cooling from the homogeneous solutions of **1**/*n*-dodecane with a concentrations ≥0.1% (w/v) the **1** molecules first undergo a solution self-assembly to form wormlike cylindrical micelles. The driving force of the assembly can be mainly attributed to the reduction of free energy during microphase separation among the different regions of molecules with distinct chemical properties and the lipophilic−lipophobic interaction in the selective solvent of the alkyl tails of **1**. The wormlike micelle is in fact a "living polymer", of which the repeating unit is the disklike molecule of **1**. In this context, the micelles belong to the simplest case of molecular threads. With lowering temperature, the length of the "living polymer" increases, allowing the chains to become entangled. The continuous "polymerization" will finally lead the micelle solution to enter the miscibility gap, and thus a solution phase separation occurs. As a dynamically asymmetric mixture, this phase separation can give a 3D network of the slow component of the **1** "living polymer", which shall be largely responsible for the gelation at low temperatures. We consider that this gelation mode can be a primitive one for the LMOGs which form gels beyond the crystallization mechanism.

The packing of **1** cylindrical micelles within the "polymer"-rich phase can produce a lyotropic rectangular ordering when the system is close to equilibrium. On the other hand, quenching or rapid cooling to a sufficiently low temperature will result in a sort of nematic packing of the "living polymers" in the gel state. The diffraction of either the rectangular or nematic ordering is substantially different from that observed from the bulk samples of **1**. As the fibers of 3D network are swollen with an amount of solvent, the gel of **1** is "wet". However, removal of the solvent will lead the "wet gel" to collapse, and the resultant xerogel renders a hexagonal packing of the **1** cylinders same as that of the bulk sample.

It is worth mentioning that the gel of **1** in fact contains two types of channels with distinct polarities and sizes: one is the hydrophobic pores of the gel network on submicrometer scale, and the other is the hydrophilic cavity of large crown ether rings aligned at the center of the **1** cylinders on the nanometer scale. Using rhodamine B as an example, we have tested the capability of the crown ether channel to accommodate guest molecules. The rhodamine B molecules can be solubilized in *n*-dodecane due to the charge-transfer interaction between the electron-rich crown ether and the ammonium in rhodamine B's structure and will be included in the crown ether channels after micellization and gelation. We expect that this type of organogel may provide considerable potentials amenable to practical applications in ion transportation, drug delivery system, filtration and separation, etc.

Acknowledgment. This work was supported by the National Nature Science Foundation of China (NNSFC Grants 20234020, 20374003, 50573001, and 20774006). The authors greatly appreciate Dr. H. Schnablegger at Anton Paar GmbH for his beneficial discussion on the SAXS data analysis.

Supporting Information Available: Synthesis and characterization of molecule **1** and UV−vis spectra of **1** in *n*-dodecane measured at various temperatures. This material is available free of charge via the Internet at http://pubs.acs.org.

References and Notes

(1) Flory, P. J. *Faraday Discuss.* **1974**, *57*, 7–18.
(2) Keller, A. *Faraday Discuss.* **1995**, *101*, 1–49.
(3) Tanaka, H. *J. Phys.: Condens. Matter* **2000**, *12*, R207–R264.
(4) George, M.; Weiss, R. G. *Acc. Chem. Res.* **2006**, *39*, 489–497.
(5) Terech, P.; Weiss, R. G. *Chem. Rev.* **1997**, *97*, 3133–3160.
(6) Langford, S. J.; Latter, M. J.; Lau, V. L.; Martin, L. L.; Mechler, A. *Org. Lett.* **2006**, *8*, 1371–1373.
(7) Gronwald, O.; Shinkai, S. *Chem.—Eur. J.* **2001**, *7*, 4328–4334.
(8) Liu, X. Y. *Top. Curr. Chem.* **2005**, *256*, 1–37.
(9) van Esch, J. H.; Feringa, B. L. *Angew. Chem., Int. Ed.* **2000**, *39*, 2263–2266.
(10) Ji, Y.; Luo, Y. F.; Jia, X. R.; Chen, E. Q.; Huang, Y.; Ye, C.; Wang, B. B.; Zhou, Q. F.; Wei, Y. *Angew. Chem., Int. Ed.* **2005**, *44*, 6025–6029.
(11) Sakurai, K.; Jeong, Y.; Koumoto, K.; Friggeri, A.; Gronwald, O.; Sakurai, S.; Okamoto, S.; Inoue, K.; Shinkai, S. *Langmuir* **2003**, *19*, 8211–8217.
(12) Yagai, S.; Iwashima, T.; Kishikawa, K.; Nakahara, S.; Karatsu, T.; Kitamura, A. *Chem.—Eur. J.* **2006**, *12*, 3984–3994.
(13) Hirst, A. R.; Smith, D. K.; Feiters, M. C.; Geurts, H. P. M.; Wright, A. C. *J. Am. Chem. Soc.* **2003**, *125*, 9010–9011.
(14) Jung, J. H.; Ono, Y.; Sakurai, K.; Sano, M.; Shinkai, S. *J. Am. Chem. Soc.* **2000**, *122*, 8648–8653.
(15) Liu, X. Y.; Sawant, P. D. *Appl. Phys. Lett.* **2001**, *79*, 3518–3520.
(16) Liu, X. Y.; Sawant, P. D. *Adv. Mater.* **2002**, *14*, 421–426.
(17) Hirst, A. R.; Coates, I. A.; Boucheteau, T. R.; Miravet, J. F.; Escuder, B.; Castelletto, V.; Hamley, I. W.; Smith, D. K. *J. Am. Chem. Soc.* **2008**, *130*, 9113–9121.
(18) Lescanne, M.; Colin, A.; Mondain-Monval, O.; Fages, F.; Pozzo, J. L. *Langmuir* **2003**, *19*, 2013–2020.
(19) Li, J. L.; Liu, X. Y.; Wang, R. Y.; Xiong, J. Y. *J. Phys. Chem. B* **2005**, *109*, 24231–24235.
(20) Liu, X. Y.; Sawant, P. D. *ChemPhysChem* **2002**, *3*, 374–377.
(21) Wang, R. Y.; Liu, X. Y.; Narayanan, J.; Xiong, J. Y.; Li, J. L. *J. Phys. Chem. B* **2006**, *110*, 25797–25802.
(22) Terech, P.; Furman, I.; Weiss, R. G. *J. Phys. Chem.* **1995**, *99*, 9558–9566.
(23) Terech, P.; Ostuni, E.; Weiss, R. G. *J. Phys. Chem.* **1996**, *100*, 3759–3766.
(24) Wang, R.; Geiger, C.; Chen, L.; Swanson, B.; Whitten, D. G. *J. Am. Chem. Soc.* **2000**, *122*, 2399–2400.
(25) Li, Y. G.; Wang, T. Y.; Liu, M. H. *Tetrahedron* **2007**, *63*, 7468–7473.
(26) Hirst, A. R.; Smith, D. K. *Top. Curr. Chem.* **2005**, *256*, 237–273.
(27) Gao, M.; Kuang, G. C.; Jia, X. R.; Li, W. S.; Li, Y.; Wei, Y. *Tetrahedron Lett.* **2008**, *49*, 6182–6187.
(28) Jang, W. D.; Aida, T. *Macromolecules* **2003**, *36*, 8461–8469.
(29) Love, C. S.; Hirst, A. R.; Chechik, V.; Smith, D. K.; Ashworth, I.; Brennan, C. *Langmuir* **2004**, *20*, 6580–6585.
(30) Jang, W. D.; Jiang, D. L.; Aida, T. *J. Am. Chem. Soc.* **2000**, *122*, 3232–3233.
(31) Percec, V.; Holerca, M. N.; Nummelin, S.; Morrison, J. L.; Glodde, M.; Smidrkal, J.; Peterca, M.; Rosen, B. M.; Uchida, S.; Balagurusamy, V. S. K.; Sienkowska, M. J.; Heiney, P. A. *Chem.—Eur. J.* **2006**, *12*, 6216–6241.
(32) Percec, V.; Cho, W.-D.; Mosier, P. E.; Ungar, G.; Yeardley, D. J. P. *J. Am. Chem. Soc.* **1998**, *120*, 11061–11070.
(33) Percec, V.; Mitchell, C. M.; Cho, W. D.; Uchida, S.; Glodde, M.; Ungar, G.; Zeng, X. B.; Liu, Y. S.; Balagurusamy, V. S. K.; Heiney, P. A. *J. Am. Chem. Soc.* **2004**, *126*, 6078–6094.
(34) Percec, V.; Heck, J. *J. Polym. Sci., Part A: Polym. Chem.* **1991**, *29*, 591–597.
(35) Percec, V.; Johansson, G.; Heck, J.; Ungar, G.; Batty, S. V. *J. Chem. Soc., Perkin Trans. 1* **1993**, 1411–1420.
(36) Zeng, X. B.; Ungar, G.; Liu, Y. S.; Percec, V.; Dulcey, S. E.; Hobbs, J. K. *Nature* **2004**, *428*, 157–160.
(37) Beginn, U.; Zipp, G.; Moller, M.; Johansson, G.; Percec, V. *Macromol. Chem. Phys.* **1997**, *198*, 2839–2852.
(38) Percec, V.; Peterca, M.; Yurchenko, M. E.; Rudick, J. G.; Heiney, P. A. *Chem.—Eur. J.* **2008**, *14*, 909–918.
(39) Percec, V.; Imam, M. R.; Peterca, M.; Wilson, D. A.; Heiney, P. A. *J. Am. Chem. Soc.* **2009**, *131*, 1294–304.
(40) Chvalun, S. N.; Shcherbina, M. A.; Yakunin, A. N.; Blackwell, J.; Percec, V. *Polym. Sci., Ser. A* **2007**, *49*, 158–167.
(41) Ungar, G.; Liu, Y. S.; Zeng, X. B.; Percec, V.; Cho, W. D. *Science* **2003**, *299*, 1208–1211.
(42) Percec, V.; Ahn, C. H.; Ungar, G.; Yeardley, D. J. P.; Moller, M.; Sheiko, S. S. *Nature* **1998**, *391*, 161–164.
(43) Beginn, U.; Zipp, G.; Moller, M. *Chem.—Eur. J.* **2000**, *6*, 2016–2023.
(44) Cates, M. E.; Candau, S. J. *J. Phys.: Condens. Matter* **1990**, *2*, 6869–6892.
(45) Scartazzini, R.; Luisi, P. L. *J. Phys. Chem.* **1988**, *92*, 829–833.
(46) Tanaka, H.; Araki, T.; Koyama, T.; Nishikawa, Y. *J. Phys.: Condens. Matter* **2005**, *17*, S3195–S3204.
(47) Jung, J. H.; Kobayashi, H.; Masuda, M.; Shimizu, T.; Shinkai, S. *J. Am. Chem. Soc.* **2001**, *123*, 8785–8789.
(48) Jung, J. H.; Lee, S. J.; Rim, J. A.; Lee, H.; Bae, T. S.; Lee, S. S.; Shinkai, S. *Chem. Mater.* **2005**, *17*, 459–462.
(49) Kawano, S. I.; Fujita, N.; Shinkai, S. *Chem. Commun.* **2003**, 1352–1353.
(50) Johansson, G.; Percec, V.; Ungar, G.; Abramic, D. *J. Chem. Soc., Perkin Trans. 1* **1994**, 447–459.
(51) Dykes, G. M.; Smith, D. K. *Tetrahedron* **2003**, *59*, 3999–4009.
(52) Lehn, J. M. *Supramolecular Chemistry: Concepts and Perspectives*; VCH: Weinheim, Germany, 1995.
(53) Ashton, P. R.; Chrystal, E. J. T.; Glink, P. T.; Menzer, S.; Schiavo, C.; Spencer, N.; Stoddart, J. F.; Tasker, P. A.; White, A. J. P.; Williams, D. J. *Chem.—Eur. J.* **1996**, *2*, 709–728.
(54) Ashton, P. R.; Fyfe, M. C. T.; Glink, P. T.; Menzer, S.; Stoddart, J. F.; White, A. J. P.; Williams, D. J. *J. Am. Chem. Soc.* **1997**, *119*, 12514–12524.
(55) Ashton, P. R.; Fyfe, M. C. T.; Schiavo, C.; Stoddart, J. F.; White, A. J. P.; Williams, D. J. *Tetrahedron Lett.* **1998**, *39*, 5455–5458.
(56) Ashton, P. R.; Glink, P. T.; Stoddart, J. F.; Tasker, P. A.; White, A. J. P.; Williams, D. J. *Chem.—Eur. J.* **1996**, *2*, 729–736.
(57) Jeong, Y.; Hanabusa, K.; Masunaga, H.; Akiba, I.; Miyoshi, K.; Sakurai, S.; Sakurai, K. *Langmuir* **2005**, *21*, 586–594.
(58) Lake, J. A. *Acta Crystallogr.* **1967**, *23*, 191–196.
(59) Glatter, O. *Acta Phys. Austriaca* **1977**, *47*, 83–102.
(60) Glatter, O. *J. Appl. Crystallogr.* **1977**, *10*, 415–421.
(61) Sakurai, K.; Ono, Y.; Jung, J. H.; Okamoto, S.; Sakurai, S.; Shinkai, S. *J. Chem. Soc., Perkin Trans. 2* **2001**, 108–112.
(62) Ostuni, E.; Kamaras, P.; Weiss, R. G. *Angew. Chem., Int. Ed.* **1996**, *35*, 1324–1326.
(63) Schaefer, D. W. *Science* **1989**, *243*, 1023–1027.
(64) Terech, P.; Allegraud, J. J.; Garner, C. M. *Langmuir* **1998**, *14*, 3991–3998.
(65) Glatter, O.; Kratky, O. *Small Angle X-ray Scattering*; Academic Press: London, 1982; p 515.
(66) Shrestha, L. K.; Sato, T.; Aramaki, K. *Langmuir* **2007**, *23*, 6606–6613.
(67) Geiger, C.; Stanescu, M.; Chen, L. H.; Whitten, D. G. *Langmuir* **1999**, *15*, 2241–2245.
(68) Schaefer, D. W.; Zhao, J.; Brown, J. M.; Anderson, D. P.; Tomlin, D. W. *Chem. Phys. Lett.* **2003**, *375*, 369–375.
(69) Terech, P.; Coutin, A. *Langmuir* **1999**, *15*, 5513–5525.
(70) Duval, M.; Waton, G.; Schosseler, F. *Langmuir* **2005**, *21*, 4904–4911.
(71) Glatter, O.; Scherf, G.; Lindner, H. *Phys. Rev. E* **2003**, *67*, 061402.
(72) Schurtenberger, P.; Cavaco, C. *Langmuir* **1994**, *10*, 100–108.
(73) Rehage, H.; Hoffmann, H. *J. Phys. Chem.* **1988**, *92*, 4712–4719.
(74) Rohatgi-Mukherjee, K. K.; Chaudhuri, R.; Bhowmik, B. B. *J. Colloid Interface Sci.* **1985**, *106*, 45–50.
(75) Ruiz, C. C.; Molina-Bolivar, J. A.; Aguiar, J.; MacIsaac, G.; Moroze, S.; Palepu, R. *Langmuir* **2001**, *17*, 6831–6840.